INSTITUTE OF PHYSICS PUBLISHING JOURNAL OF PHYSICS B: ATOMIC, MOLECULAR AND OPTICAL PHYSICS

J. Phys. B: At. Mol. Opt. Phys. **38** (2005) 3673–3685 doi:10.1088/0953-4075/38/20/004

Production of large molecular ion crystals via sympathetic cooling by laser-cooled Ba^+

B Roth, A Ostendorf, H Wenz and S Schiller

Institut für Experimentalphysik, Heinrich-Heine-Universität Düsseldorf, 40225 Düsseldorf, Germany

Received 17 March 2005, in final form 2 August 2005
Published 26 September 2005
Online at stacks.iop.org/JPhysB/38/3673

Abstract

We have produced ensembles of cold $^{16}O_2^+$, $^{40}Ar^+$, $^{12}C^{16}O_2^+$, and various isotopes of barium ions ($^{135}Ba^+$, $^{136}Ba^+$ and $^{137}Ba^+$) via sympathetic cooling with laser-cooled $^{138}Ba^+$ in a linear radiofrequency trap. The sympathetically cooled species were embedded in the centre of large $^{138}Ba^+$ Coulomb crystals containing up to 2000 ions and were identified by motional resonance excitation. Crystals with molecular fractions exceeding 70% were obtained. The observed multi-species crystal structures agree well with results from molecular dynamics simulations. The simulations were also used to deduce an upper limit for the translational temperature of the molecular ions, as low as 20 mK.

(Some figures in this article are in colour only in the electronic version)

1. Introduction

Cold pure and mixed-species ion plasmas with translational temperatures in the millikelvin range are attractive systems for quantum optics, molecular physics, fundamental physics, precision metrology and chemical physics [1–14]. The wide range of possible applications calls for the development of methods for reliable and reproducible samples of cold atomic and molecular ion species with well-characterized composition. Direct cooling methods, such as laser cooling, successfully used for numerous neutral atoms and atomic ions, cannot be easily applied to many atomic species due to the limited range of laser sources available. Laser cooling of molecules is not feasible due to the lack of closed optical transitions. A powerful method for the (indirect) cooling of a wide variety of atomic and molecular ions, independent of their internal level structure, is sympathetic cooling [8, 9, 11]. Here, particles of one species are cooled by an ensemble of directly cooled, usually laser-cooled, atoms via their mutual interaction. The absence of closed transitions in molecules also implies that fluorescence detection will typically not be applicable, so that alternative techniques are required for the identification of sympathetically cooled species [14–16].

Sympathetic cooling of several species of atomic ions was achieved by using laser-cooled $^{9}Be^{+}$ [5], $^{24}Mg^{+}$ [17–19], $^{40}Ca^{+}$ [20] and $^{114}Cd^{+}$ [21] as coolants, in both Penning and radiofrequency traps. Cold molecular ions (MgH^{+}) have been formed by reactions of H_2 with optically excited Mg^{+}, sympathetically cooled, and their photo-dissociation studied [8, 10, 22]. Cold BeH^{+} and BeD^{+} ions have been produced in a similar way [7]. Recently, we have demonstrated reliable production of cold molecular hydrogen isotopomers and helium isotopes, via sympathetic cooling with laser-cooled Be^{+} in a linear Paul trap [5, 23]. Chemical reactions between sympathetically cooled particles and neutral reactants were studied, using $^{138}Ba^{+}$ as a coolant [15]. Extraction of the product ions from the trap and detection was demonstrated for small $^{138}Ba^{+}$ ion crystals containing sympathetically cooled species. However, sympathetic cooling of ions in large $^{138}Ba^{+}$ crystals has not been reported so far.

In this work, we report the production of large $^{138}Ba^{+}$ ion crystals in a linear Paul trap containing up to 2000 particles. Up to 250 $^{16}O_2^{+}$, $^{40}Ar^{+}$ and $^{12}C^{16}O_2^{+}$ ions were sympathetically cooled and embedded inside the cold crystallized structures. In addition, other barium isotopes, $^{135}Ba^{+}$, $^{136}Ba^{+}$ and $^{137}Ba^{+}$, and molecular ions, such as $^{138}Ba^{16}O^{+}$, produced by chemical reactions with residual gas molecules, were sympathetically cooled and crystallized. We identified trapped ion species by excitation of their oscillation modes and determined their temperature.

2. Experiment

A linear radio frequency ion trap (Paul trap) is used to simultaneously store the atomic coolant ($^{138}Ba^{+}$) and the sympathetically cooled particles. The trap is enclosed in an ultra-high vacuum chamber at below 1×10^{-10} mbar. Neutral gases can be introduced into the chamber via a leak valve. The linear Paul trap consists of four cylindrical electrodes, each sectioned longitudinally into three parts. The overall length of the electrodes is 10 cm, the central trapping region being 2 cm long. Stable trapping of $^{138}Ba^{+}$ is achieved with a Mathieu stability parameter, $q\left(=2QV_{\mathrm{RF}}/m\Omega^2 r_0^2\right) \approx 0.05$, with Q and m being the atomic charge and mass, respectively. V_{RF} and Ω are the amplitude and frequency of the rf driving field and $r_0 = 4.3$ mm is the distance from the trap centre to the electrodes. The radial (transverse) confinement of the ions is achieved by applying an rf drive at a frequency Ω of $2\pi \times 2.9$ MHz and an amplitude of up to 800 V to the trap electrodes. For the sympathetically cooled particles studied here this gives a stability parameter q in the range 0.05–0.15. The effective trap potential is given by

$$U_{\mathrm{trap}}(x, y, z) = \frac{m}{2}\left(\omega_r^2(x^2 + y^2) + \omega_z^2 z^2\right), \tag{1}$$

with the z-axis along the trap centreline. The transverse oscillation frequency is

$$\omega_r = \left(\omega_0^2 - \omega_z^2/2\right)^{1/2}, \tag{2}$$

with $\omega_0 = QV_{\mathrm{RF}}/\sqrt{2}m\Omega r_0^2$. In the longitudinal direction, the oscillation frequency is given by $\omega_z = (2\kappa QV_{\mathrm{EC}}/m)^{1/2}$, where V_{EC} is a static potential added to the eight end sections (endcaps) of the electrodes to ensure confinement along the z-axis. The factor $\kappa \approx 3 \times 10^{-3}$ mm^{-2} is a constant determined by the trap geometry.

$^{138}Ba^{+}$ ions are laser cooled on the $6^2S_{1/2} \rightarrow 6^2P_{1/2}$ transition at 493.4 nm. In addition, a repumper laser at 649.8 nm is necessary to prevent optical pumping to the metastable $5^2D_{3/2}$ state. In our set-up, the cooling laser radiation is generated by non-resonant sum frequency generation (SFG) of two solid-state lasers, a single frequency Nd:YAG laser at 1064 nm with an output power of 6 W and a Ti:Sapphire laser with 700 mW at 920 nm, in a periodically poled KTP crystal. Absolute frequency stability of the Nd:YAG laser is provided by frequency

doubling a small part of the laser radiation and locking to a line of the sub-Doppler hyperfine spectrum in iodine via modulation transfer spectroscopy. The Ti:Sapphire laser has a built-in reference cavity for stabilization. Output powers of 40 mW were achieved with this set-up. As a repumper, an external cavity laser diode at 649.8 nm was used with an output power of ∼10 mW. The linewidth of the repumper laser was measured to be 300 kHz, via cavity ring-down spectroscopy in a monolithic bow-tie cavity. For laser cooling of the barium ions, the two laser beams are linearly polarized in the vertical direction (transverse to the z-axis) and propagate along z. The effect of radiation pressure force on the produced cold ion plasmas is reduced, if required, by using two counterpropagating cooling laser beams. To maintain fluorescence, magnetic fields in the few gauss range are applied to the trap. The direction of the magnetic field is parallel to z.

For loading the trap, neutral atoms are evaporated from a barium oven and ionized *in situ* by a 500 eV electron beam crossing the trap centre. During Ba^+ loading, the cooling and repumper lasers are manually set to a frequency red detuned from the atomic resonance by several natural linewidths. The $^{138}Ba^+$ fluorescence is simultaneously recorded with a photomultiplier and an intensified CCD (ICCD) camera. A magnification of 10 was chosen for the imaging system of the ICCD camera.

For strong cooling, the Ba^+ ion cloud undergoes a phase transition from the fluid ion plasma to an ordered state, a Coulomb crystal. This phase transition reveals itself by a sudden increase in the detected fluorescence level, caused by the reduction in the particle velocities, and the consequently smaller Doppler broadening. Once the phase transition occurs, the frequencies of the lasers are adjusted for maximum cooling rate, controlled via continuous imaging of the cold ion plasma using the ICCD. The generated ion crystals are stable under these conditions, provided that the temperature stability of the laser environment is sufficiently stable. Typical storage times are in the range of a few hours. No significant particle losses were observed even when the laser radiation was blocked or strongly detuned for several minutes, see also [24].

If necessary, mass-selective cleaning of the trap is applied to eject heavy impurity particles, e.g. BaO^+, formed by chemical reactions during loading. To this end, we add a static quadrupole potential V_{DC} to the trap until the a-parameter $\left(a = 4QV_{DC}/m\Omega^2 r_0^2\right)$ of the unwanted species lies outside the Mathieu stability range [25]. Thus, stable trapping of particles exceeding the mass of the atomic coolants is prevented.

3. Molecular dynamics simulations

In the simulations we solve Newton's equations of motion for laser-cooled and sympathetically cooled ions in the quasi-potential approximation

$$m_i\ddot{\mathbf{x}}_i = Q_i\nabla(U_{\text{trap}}(\mathbf{x}_i)) + \mathbf{F}_{C,i}(\{\mathbf{x}_j\}) + \mathbf{F}_{\mathbf{L}}(\dot{\mathbf{x}}_i), \tag{3}$$

where $i = 1, \ldots, N_{LC} + N_{SC}$. N_{LC} and N_{SC} are the number of laser-cooled (LC) and sympathetically cooled (SC) ions, respectively. m_i, Q_i and $\mathbf{x}_i = (x_i, y_i, z_i)$ are the masses, charges and positions of the particles. $\mathbf{F}_{C,i}(\{\mathbf{x}_j\}) = (Q_i/4\pi\epsilon_0)\nabla_i \Sigma_j Q_j/r_{ij}$ is the Coulomb force and r_{ij} is the distance between two ions. Trap asymmetries due to electric offset potentials are added to the quasi-potential U_{trap}. For simplicity, simulations are performed using a continuous linear viscous damping force $\mathbf{F}_{\mathbf{L}} = -\beta\dot{\mathbf{x}}_i$ in the horizontal direction. The friction coefficient β is chosen well below the maximum value for transitions at optical wavelengths [26]. We have used stronger cooling forces $\mathbf{F}_{\mathbf{L}}$ to speed up cooling. Micromotion is not included because it is not expected to be important for the crystals presented here (see also section 4.4).

The equations of motion are numerically solved using the Leapfrog algorithm which is computationally less expensive than other methods, e.g. the higher-order Runge–Kutta algorithm. Moreover, the conservation of energy is respected, even at large time steps. Sympathetic cooling by laser-cooled $^{138}Ba^{+}$ can be simulated for up to four ion species. Heating processes for particular species can be added. In order to produce simulated images for a comparison with CCD images, projections of the particle positions on the observation plane are generated for a time series and superimposed.

4. Results

4.1. Barium ion crystals

Figure 1 shows several Ba^{+} ion crystals, (a), (b), (d) and (f), together with results from molecular dynamics (MD) simulations, (c) and (e). The prolate crystal in figure 1(a) is a typical example of a large barium ion crystal obtained with our apparatus. The cooling laser frequency was adjusted for maximum cooling power. The crystal contains ≈2000 laser-cooled (LC) $^{138}Ba^{+}$ and ≈1000 sympathetically cooled (SC) barium isotopes. It has an overall length of ≈2 mm along the z-axis and an extension of ≈0.1 mm in the vertical direction.

Figure 1(b) shows a medium-sized mixed-species barium crystal containing ≈200 $^{138}Ba^{+}$ and ≈100 other barium isotopes ($^{135}Ba^{+}$, $^{136}Ba^{+}$ and $^{137}Ba^{+}$). Due to light pressure forces on the LC particles the SC ions are located on the left end of the crystal, see also [9].

In figure 1(c) the result of MD simulations for the ion crystal shown in (b) is presented. In the simulations, the number of ions is varied until the observed crystal structure is reproduced. Typical observed radial intershell spacings for the LC ions are ≈19 μm, in good agreement with the value obtained from the MD simulations.

The influence of SC-cooled particles and light pressure forces on the formed crystal structures is illustrated in figures 1(d)–(f). Figures 1(d), (e) show an ion string. As is well known, the ion distances increase away from the string centre. For this string, the spacing between adjacent $^{138}Ba^{+}$ ions varies between 31 μm and 55 μm. The string contains 20 $^{138}Ba^{+}$ and approximately ten other barium isotopes, located at the left end of the crystal, as obtained from the simulations, figure 1(e). Occasionally, the ions collide with neutral background gas or hot ions present in the trap. Thus, individual ions may be kicked out of their position in the string, then re-cooled and again embedded in the crystal, but at a different position [9]. This is the case for the single $^{138}Ba^{+}$ ion on the left end of the crystal in figure 1(d) where random jumps were observed. For a different crystal structure, figure 1(f), where the LC (and SC) ions are arranged in a zig-zag configuration, the observed pitch varies between ≈27 μm and ≈34 μm.

4.2. Micromotion reduction

The images of the Coulomb crystals in figure 1, in particular the outermost regions (in the radial direction) of the large structures, are blurred. This is attributed to residual micromotion, depending on the distance of the particles from trap centre and the symmetry of the effective trap potential. The distortion of the effective potential is mainly due to stray fields and the partial coating of the trap electrodes during evaporation of neutral barium from the oven. By adding additional static offset potentials to the central trap segments, the distortion can be compensated. A direct measurement of the micromotion can be obtained by correlating the fluorescence rate of the atomic coolants to the rf amplitude of the trap [27]. For our set-up, the photomultiplier (PMT) count rate is typically smaller than the rf field frequency (≈1 MHz

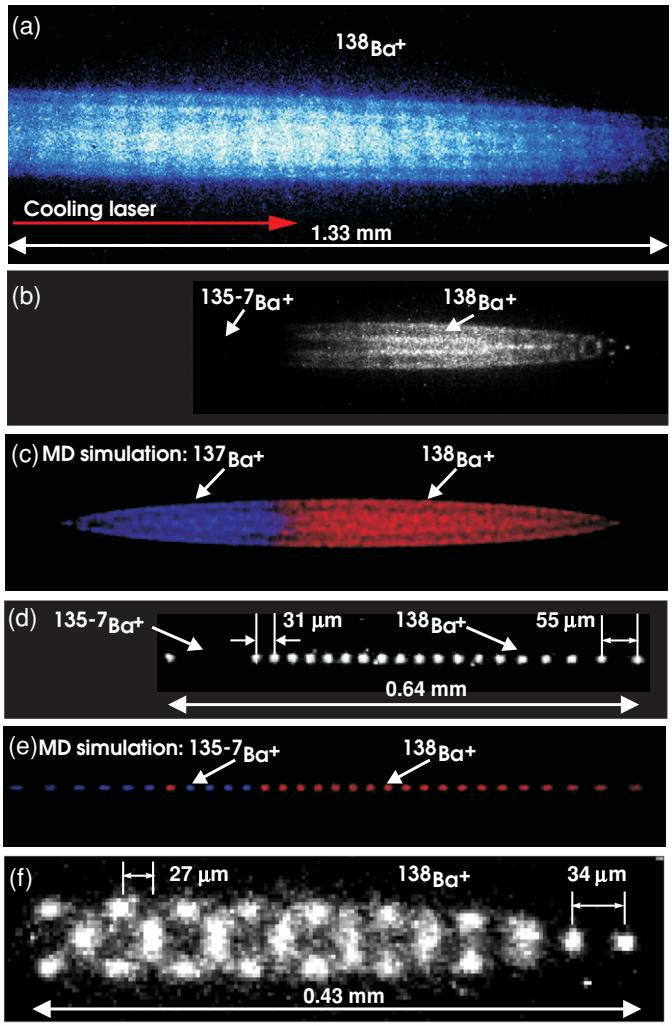

Figure 1. ICCD camera images of different $^{138}Ba^+$ crystals. The cooling and repumper laser beam directions are to the right. Camera integration time was 1 s. (a) Large Coulomb crystal containing ≈2000 $^{138}Ba^+$ ions and ≈1000 sympathetically cooled (SC) barium isotopes, located on the left side of the crystal. (b) ion crystal containing ≈200 $^{138}Ba^+$ and ≈100 other barium isotopes, predominantly $^{137}Ba^+$ and smaller admixtures of $^{135}Ba^+$ and $^{136}Ba^+$. (c) MD simulation of the crystal shown in figure 1 (b). LC ions, $^{138}Ba^+$: red, SC ions, $^{137}Ba^+$: blue. The translational temperature for LC and SC ions is approximately 20 mK, according to the simulations. (d) ion string consisting of 20 $^{138}Ba^+$ ions and eight other barium isotopes. The location of the SC ions is marked by arrows. (e) MD simulation of the ion string in (d). (f) Zig-zag structure of a Ba^+ ion crystal. The indicated dimensions are measured after calibration of the optical system.

versus $\Omega/2\pi = 2.75$ MHz, for this measurement). The PMT provides the start trigger pulse for a time-to-amplitude converter (TAC 567, EG&G Ortec). The stop pulse is provided by the zero crossing (or a slope) of the rf field. A multi-channel-analyser (MCA 917, EG&G Ortec) bins the counts according to the time delay between the start and the stop pulse.

The result of such a correlation measurement is shown in figure 2. Typically, for the recorded count rate, one obtains a single oscillation with a period $\sim 2\pi/\Omega$ and an amplitude proportional to the micromotion amplitude. The modulation amplitude was reduced by a

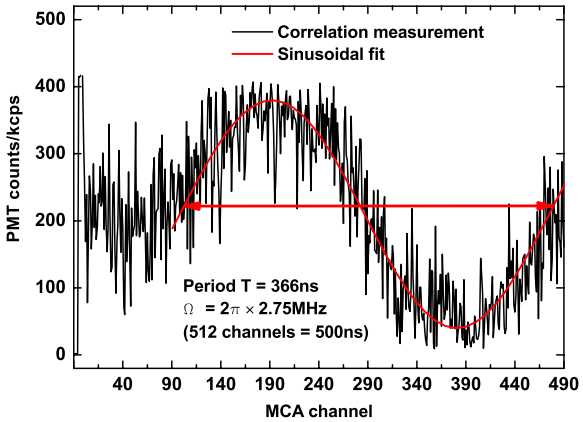

Figure 2. Correlation of the fluorescence emission rate with trap modulation, detected with a PMT in photon count mode. The initial part of the fluorescence curve (MCA channels 0–90) is flattened due to electronic noise.

factor of ≈2 by adding static offset potentials of up to 0.2 V to the central electrodes. This led to sharper ICCD images. In order to minimize or eliminate the micromotion excitation in all dimensions, a more complicated set-up involving three laser beams is required [27].

4.3. Sympathetic cooling and crystallization

4.3.1. BaO^+. Cold $^{138}BaO^+$ molecular ions were produced by chemical reactions with background CO_2 molecules evaporated from the filaments of the electron gun and the barium oven:

$$Ba^+ + CO_2 \longrightarrow BaO^+ + CO. \tag{4}$$

This reaction is exothermic by several eV [28–30]. Direct formation of BaO^+ via the reaction $Ba^+ + O_2 \longrightarrow BaO^+ + O$ is precluded by its (measured) endothermicity even with optically excited Ba^+, see [31], apart from the negligible partial pressure of oxygen in our chamber. Similarly, chemical reactions between ground state and excited state Ba^+ and neutral H_2 gas, also present in the ultra-high vacuum system, are also endothermic by several eV, see [29], and therefore do not occur under our experimental conditions. These facts were verified by exposing large barium ion crystals to neutral hydrogen or oxygen gas, where no chemical reactions could be observed for typical exposure times of several minutes.

As shown in figure 3(a), the BaO^+ ions are located in the outer shell of the crystal. According to our simulations, (figure 3(b)), the crystal contains ≈250 $^{138}Ba^+$, 125 $^{135-7}Ba^+$ and 100 $^{138}BaO^+$ ions. The substantial formation of BaH^+ ions can be excluded, since the simulated structures, (figure 3(c)), are in clear disagreement with the observed ones. In particular, the simulations show how the light force causes the BaH^+ ions being located more on the left part of the crystal, together with the other barium isotopes, due to the similarity of mass. Furthermore, the shape of the crystal structure has changed. Whereas in the presence of SC BaO^+, the outermost $^{138}Ba^+$ ion shell has a flat shape over the whole length of the crystal, the longitudinal separation between $^{138}Ba^+$ and $^{138}BaH^+$ ions in figure 3(c) is more pronounced and abrupt, not observed in experiment (figure 3(a)). The location of the molecular ions on the lower side of the crystal is caused by small asymmetries of the effective trap potential, taken into account in the simulations. The laser-cooled and sympathetically cooled particles have a translational temperature of ≈20 mK, see below. The right end of the experimental structure

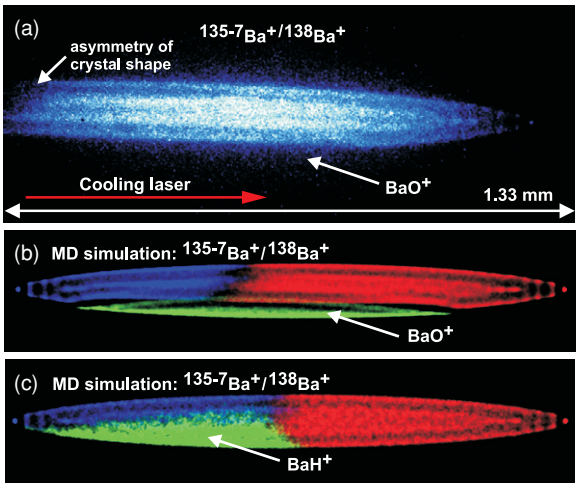

Figure 3. (a) Multi-species crystal of approximately 250 $^{138}Ba^+$, 125 $^{135-7}Ba^+$ and 100 $^{138}Ba^{16}O^+$ ions. The particle numbers were obtained from a MD simulation (b) that reproduced the observed crystal. (c) MD simulation of the multi-species ion crystal from (b) where $^{138}Ba^1\,H^+$ ions instead of $^{138}Ba^{16}O^+$ ions were used.

in figure 3(a) appears tilted. This is caused by sympathetically cooled barium isotopes and, again, by small asymmetries of the effective trap potential, leading to a displacement of the ions from the centre of the trap, as confirmed by the simulations (figure 3(b)).

4.3.2. Light molecular ions. After large barium ion crystals were formed and purified as described above, $^{16}O_2^+$, $^{40}Ar^+$ and $^{12}CO_2^+$ ions were produced by leaking O_2, Ar or CO_2 gas into the vacuum chamber at a partial pressure of 10^{-8} mbar and ionizing it *in situ* in the trap by a 200 eV electron beam. The loading rate was controlled by the partial pressure of the neutral gas and the electron beam intensity. As a consequence of sympathetic cooling and crystallization of the molecular ions, a dark inner region evolves in the initially pure crystals. According to equation (1), the lighter molecular species experience a stronger effective potential and are therefore embedded closer to the z-axis of the trap. As an example, a cold multi-species ion crystal containing $^{138}Ba^+$, $^{135-7}Ba^+$, $Ba^{16}O^+$, $^{40}Ar^+$ and $^{12}C^{16}O_2^+$ is shown in figure 4(a). Using the simulations the number of LC (≈300) and SC-cooled particles (≈590) were deduced. For simplicity, the simulations were run with a single lighter SC ion species of mass = 42. With these numbers the resulting crystal structures were modelled for different translational temperatures of the $^{138}Ba^+$ (see below). Agreement between the predicted and the observed crystal structure is achieved for a translational temperature of ≈20 mK for $^{138}Ba^+$, the temperature of the SC ions being very similar, figure 4(b).

4.4. Crystal temperature

Upper limits for the translational temperatures of the LC and SC ions in crystals of arbitrary shape and composition can be deduced from MD simulations. The size of the ion fluorescence spots in the ICCD images is compared to the simulation results performed for a range of temperatures. Figures 5(a)–(d) show the computed spatial distribution as a function of temperature for an ion crystal containing 360 $^{138}Ba^+$ and 180 atoms of the barium isotopes $^{135}Ba^+$, $^{136}Ba^+$ and $^{137}Ba^+$. The corresponding experimental ion crystal, figure 5(e), is consistent with a temperature between 4 and 10 mK (the $^{138}Ba^+$ Doppler temperature is

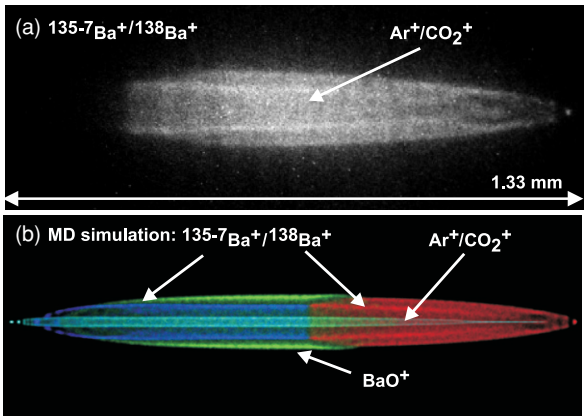

Figure 4. (a) Multi-species ion crystal following loading with a mixture of Ar and CO_2 gas, containing ≈300 $^{138}Ba^+$ (red), ≈150 barium isotopes (blue, embedded on the left end of the crystal), ≈240 $^{138}Ba^{16}O^+$ ions (green, located in the outermost shells) and ≈200 $^{40}Ar^+$ plus $^{12}C^{16}O_2^+$ ions in approximately equal proportions (light blue, embedded around the z-axis). The lighter SC particles were identified via motional resonance excitation, see below. The asymmetry of the ion crystal in the horizontal direction (along the z-axis) is due to light pressure forces. (b) MD simulation of the crystal shown in figure 4(a). The simulations show the whole crystal and are thus not to scale with the experimental images.

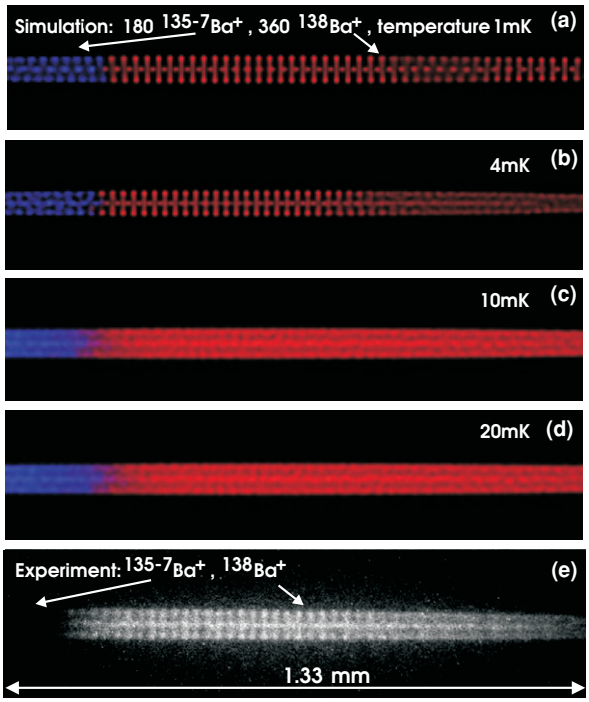

Figure 5. Comparison between simulated (a)–(d) and measured (e) Ba^+ ion crystal structures. In the simulations, the translational temperature of the Ba^+ crystal was varied. Note that (e) is magnified compared to (a)–(d).

0.15 mK). The obtained estimate for the LC particles is consistent with direct temperature measurements we performed, see also [32, 33, 5, 18]. Because of the Coulomb coupling between LC and SC ions, the temperature of the latter influences the former. Because of this we can infer information about the SC ion temperature from the LC ion temperature, which is manifested through the CCD images. For example, if in the simulations of light ions (e.g. O_2^+, Ar^+, CO_2^+) embedded in the centre of the ion crystal they are kept at a temperature >50 mK (by adding a heating source), the Ba^+ ion spots surrounding the molecular ions are much more blurred than observed experimentally. Similarly, for the case of BaO^+ ions located at the edge of a Ba^+ crystal, the observed Ba^+ ion spot size in the outermost shell is inconsistent with a BaO^+ temperature >50 mK. Tighter upper limits can be set by stimulating the balance between heating and cooling rates for the SC particles. The cooling is provided by the LC particles kept at a constant temperature chosen so that simulated and measured images agree. Heating occurs due to collisions with background particles and due to rf heating. Rf heating is negligible for crystals at $\ll 1$ K and small q. This has been shown both experimentally [24] and by MD simulations [34, 35]. The background collision heating rate was estimated at ≈ 1 K/particles from experimental observations of random jumps of individual Ba^+ ions, induced by collisions, in small mixed-species crystals. The relevant cooling rates were extracted from the simulations (see also [36]). We find, both for SC particles in the centre and for heavy SC particles at the Ba^+ crystal boundary that the SC ion temperature is at most not larger than a factor of 2 of the Ba^+ temperature. Our results do not indicate a major effect on the SC temperature due to the significantly different mass ratio m_{SC}/m_{LC} for the two cases [37].

Furthermore, for the crystals shown, small asymmetries of the trap potential lead to a good coupling between longitudinal and radial degrees of freedom of the Ba^+ ions, and thus, also to more efficient sympathetic cooling rates. This was checked by carefully aligning the laser beams along the trap symmetry axis which leads to a reduced coupling between, and therefore, to a reduced cooling rate for the radial degrees of freedom of LC (and SC) ions. Experimentally, this becomes obvious from a more blurred shell structure of the ion crystal, induced by an uncorrelated rotation-like diffusion of the ions around the trap symmetry axis, also seen in the simulations.

4.5. Mass spectroscopy

The trapped ion species are identified by excitation of their motion in the radial direction. For this purpose, a low-frequency rf field is added with opposite phase to the two orthogonal pairs of the central electrodes. When the frequency of the excitation field is resonant with a mode frequency of a trapped ion species the $^{138}Ba^+$ fluorescence level changes. This is due to heating of the excited ion species, which in turn leads to heating of the LC ions via Coulomb interaction, and thus to a change of the observed fluorescence. For the large crystals studied here, this method allows for the identification of trapped ion species when the relative difference between their mass-to-charge ratios m/q is larger than $\approx 10\%$. For a single molecular ion trapped and sympathetically cooled by a single atomic ion, very high q/m resolution in the 10^{-4} range can be achieved, see [16].

For $\omega_0 \gg \omega_z$, the radial oscillation frequency for a single trapped SC ion with mass m_{SC} is approximately given by

$$\omega_{r,SC} = \frac{m_{Ba}}{m_{Sc}} \omega_{r,Ba}, \tag{5}$$

with $\omega_{r,Ba}$ (m_{Ba}) being the corresponding radial oscillation frequency (mass) of $^{138}Ba^+$. The shape of the observed secular spectra depends strongly on the applied excitation amplitude and the laser cooling rates, see e.g. [15, 38, 39].

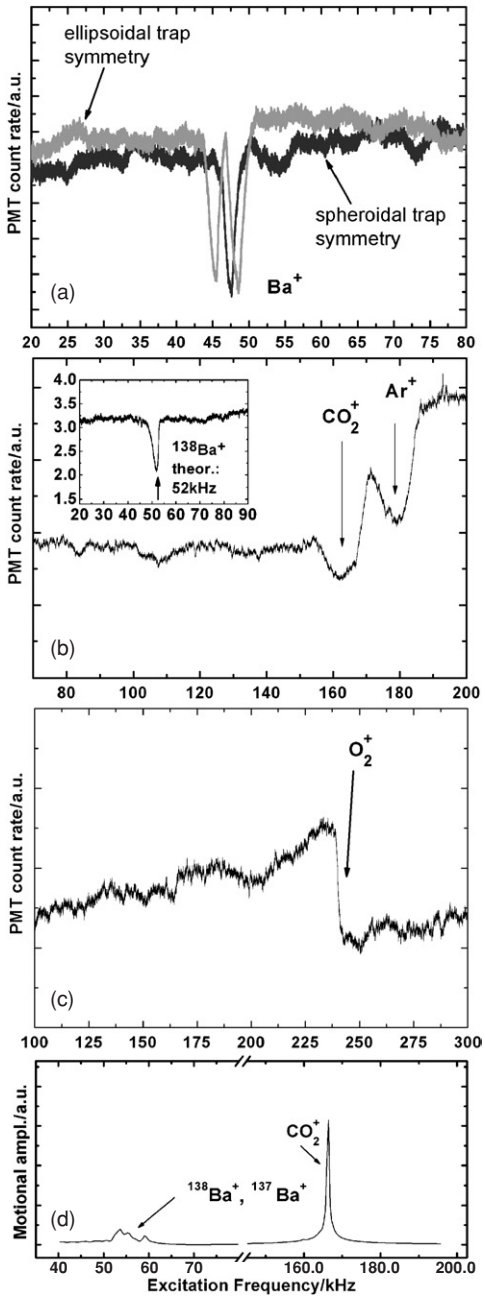

Figure 6. (a) Motional resonance spectrum for a barium ion crystal. Individual resonances for the different barium isotopes were not resolved. Secular excitation amplitude: 0.1 V. Sweep directions: towards higher frequency. Black (grey) line: for spheroidal (ellipsoidal) symmetry of the trap potential. (b) Motional spectrum for the crystal displayed in figure 4(a). Secular excitation amplitude: 0.2 V. The inset shows the measured barium resonance frequency for that crystal. (c) Motional spectrum following loading of O_2. Modulation amplitude: 0.2 V. (d) Motional resonance spectrum for a three-component ion crystal containing $^{138}Ba^+$, $^{137}Ba^+$ and $^{12}C^{16}O_2^+$, as obtained from MD simulations. The simulated crystal is comparable in size, shape and contained ion number to the crystal in figure 4(a).

Figure 6 displays four motional resonance spectra obtained for different ion crystals. The different barium isotopes were not resolved. Figure 6(a) shows the result obtained for an ion crystal containing only barium, and figures 6(b), (c) show spectra for cold multi-component ion crystals. In the latter, relatively large excitation amplitudes were applied, thereby ejecting a certain fraction of ions with each sweep, and the size of the dark crystal core was reduced with repeated excitation sweeps. For a symmetric trap potential, the expected single-particle motional frequency of the $^{138}Ba^+$ is 46 kHz, in good agreement with the experimental result. Figure 6(a) also shows a measurement of the motional spectrum for a non-radially symmetric trap potential (grey line), obtained by applying static quadrupole voltages V_{DC} of $\approx$10 mV to the central electrodes. In this case, the degeneracy between the transverse oscillation modes (with respect to the x and y axes) is removed. The transverse frequencies are then given by $\omega_{x,y}^2 = Q^2 V_{RF}^2 / (2m^2\Omega^2 r_0^4) - \omega_z^2/2 \pm Q V_{DC}/m r_0^2$. Since for $V_{DC} = 0$, ω_x and ω_y are degenerate, motional resonance excitation can be used as an indicator for compensation of stray fields.

The observed motional frequencies depend on various parameters. For example, the frequency sweep direction during excitation (from low-to-high or opposite) and the excitation amplitude induce a systematic shift of the motional frequencies. A detailed discussion of these line shifting effects can be found in e.g. [38, 39]. Furthermore, line shifts in the motional spectra are induced by coupling between different ion species in the trap, via their Coulomb interaction, which can lead to significant deviations between the measurement and the value of equation (5), which is a single-particle property [39]. In particular, the coupling between $^{138}Ba^+$ and sympathetic particles leads to a shift of all measured frequencies to higher values. However, for the spectra shown in figures 6(b), (c) the upward shift of the frequencies was compensated by a large excitation amplitude, the latter leading to an opposite shift of the resonance frequency (for a sweep direction towards higher frequencies). In the spectra in figures 6(b), (c) significant changes in the barium fluorescence were found for $\approx$160 kHz, $\approx$180 kHz (b) and $\approx$230 kHz (c), which can be attributed to the excitation of cold and crystallized $^{12}C^{16}O_2^+$, $^{40}Ar^+$ and $^{16}O_2^+$, respectively. The net result of the two compensating effects are frequency values close to the single-particle values of 163 kHz for $^{12}C^{16}O_2^+$, 179 kHz for $^{40}Ar^+$ and 224 kHz for $^{16}O_2^+$.

Using the MD simulations, the motional frequency spectrum for pure and mixed-species ion crystals can be computed. As an initial condition, the positions of all particles of a simulated crystal are shifted in the x-direction. Subsequently, the particles perform damped oscillations around their equilibrium positions. The Fourier transform of the sum of the x-coordinates of each species is computed. It can be regarded as an indicator of the resonance spectrum for periodic excitations, as performed experimentally. The computed motional frequency spectrum for a three-component ion crystal containing $^{138}Ba^+$, $^{137}Ba^+$ and $^{12}C^{16}O_2^+$ ions is shown in figure 6(d). The obtained frequency for the $^{12}C^{16}O_2^+$ (166 kHz) is in good agreement with the measured value at 160 kHz (figure 6(b)). Furthermore, in the simulations different barium isotopes, such as $^{138}Ba^+$ and $^{137}Ba^+$, can be resolved. The motional frequencies of the three ion species are in good agreement with the values of equation (5). Note that for the simulation of the $^{12}C^{16}O_2^+$ motional spectrum, a larger excitation amplitude compared to that used for simulating the motional spectrum of the barium isotopes was applied.

5. Summary

In summary, we have employed sympathetic cooling by laser-cooled $^{138}Ba^+$ to produce cold, mixed-species ion crystals containing large fractions of $^{16}O_2^+$, $^{40}Ar^+$, $^{12}C^{16}O_2^+$, and various barium isotopes ($^{135}Ba^+$, $^{136}Ba^+$ and $^{137}Ba^+$). Large Coulomb crystals of up to 2000

particles were formed with translational temperatures as low as approximately 20 millikelvin. The ion species were identified by motional resonance excitation. Molecular dynamics simulations were performed for reproducing the observed mixed-species crystal structures and for modelling the motional resonance spectra. Good agreement was found between experimental and theoretical results for the shape of the ion crystals produced. The positions of the measured and simulated motional resonance frequencies agree with an accuracy of a few per cent. Moreover, the MD simulations allowed the estimation of the translational temperature of the ion species.

Cold multi-species ion plasmas are interesting systems for a broad field of research ranging from cold chemistry to precision measurements in fundamental physics. The obtained results represent a starting point for the sympathetic cooling of highly charged atomic ions [36], using a rf trap, and the extension of sympathetic cooling to complex molecules, e.g. proteins or polymers, with masses of many thousand amu [26].

Acknowledgments

We acknowledge support from the Deutsche Forschungsgemeinschaft (DFG) in the framework of SPP1116 and the EU network 'Cold Molecules' HPRN-CT-2002-00290.

References

[1] Schmidt-Kaler F *et al* 2003 Realization of the Cirac–Zoller controlled-NOT quantum gate *Nature* **422** 408–11
[2] Chiaverini J *et al* 2004 Realization of quantum error correction *Nature* **432** 602–5
[3] Karshenboim S G and Ivanov V G 2002 Hyperfine structure of the ground and first excited states in light hydrogen-like atoms and high-precision tests of QED *Eur. Phys. J.* D **19** 13–23
[4] See, e.g., Wineland D J *et al* 2002 *Proc. 6th Symp. on Freq. Standards and Metrology* ed P Gill (Singapore: World Scientific) pp 361–8
[5] Roth B *et al* 2005 Sympathetic cooling of $^4He^+$-ions in a radiofrequency trap *Phys. Rev. Lett.* **94** 053001
[6] Schiller S and Korobov V I 2005 Test of time-independence of the electron and nuclear masses with ultracold molecules *Phys. Rev.* A **71** 032505
[7] Fröhlich U, Roth B, Antonini P, Lämmerzahl C, Wicht A and Schiller S 2004 Ultracold trapped molecules: novel systems for test of the time-independence of the electron-to-proton mass ratio *Springer Lect. Notes Phys.* **648** 297–307
[8] Molhave K and Drewsen M 2000 Formation of translationally cold MgH^+ and MgD^+ molecules in an ion trap *Phys. Rev.* A **62** 011401(R)
[9] Bowe P, Hornekaer L, Brodersen C, Drewsen M, Hangst J S and Schiffer J P 1999 Sympathetic crystallization of trapped ions *Phys. Rev. Lett.* **82** 2071
[10] Bertelsen A *et al* 2004 Photo-dissociation of cold MgH^+ ions *Eur. Phys. J.* D **31** 403–8
[11] Larson D J, Bergquist J C, Bollinger J J, Itano Wayne M and Wineland D J 1986 Sympathetic cooling of trapped ions: a laser-cooled two-species nonneutral ion plasma *Phys. Rev. Lett.* **57** 70
[12] Drullinger R E, Wineland D J and Bergquist J C 1980 High-Resolution optical spectra of laser cooled ions *Appl. Phys.* **22** 365
[13] Glenewinkel-Meyer T and Gerlich D 1997 Single and merged beam studies of the reaction H_2^+ ($v = 0, 1$; $j = 0, 4$) + $H_2^+ \rightarrow H_3^+ + H$ *Isr. J. Chem.* **37** 343–52
[14] Welling M *et al* 1998 Ion/molecule reactions, mass spectrometry and optical spectroscopy in a linear ion trap *Int. J. Mass. Spectrom. Ion Process.* **172** 95–114
[15] Baba T and Waki I 2001 Laser-cooled fluorescence mass spectrometry using laser-cooled barium ions in a tandem linear trap *J. Appl. Phys.* **89** 4592
[16] Drewsen M *et al* 2004 Nondestructive identification of cold and extremely localized single molecular ions *Phys. Rev. Lett.* **93** 243201
[17] Hasegawa T and Shimizu T 2002 Resonant oscillation modes of sympathetically cooled ions in a radio-frequency trap *Phys. Rev.* A **66** 063404
[18] van Eijkelenborg M A, Storkey M E M, Segal D M and Thompson R C 1999 Sympathetic cooling and detection of molecular ions in a penning trap *Phys. Rev.* A **60** 3903

[19] Imajo H *et al* 1996 High-resolution ultraviolet spectra of sympathetically-laser-cooled Cd^+ ions *Phys. Rev.* A **53** 122–5
[20] Kai Y *et al* 2001 Motional resonances of sympathetically cooled $^{44}Ca^+$, Zn^+, or Ga^+ ions in a linear Paul trap *Japan. J. Appl. Phys.* **40** 5136–40
[21] Blinov B B *et al* 2002 Sympathetic cooling of trapped Cd^+ isotopes *Phys. Rev.* A **65** 040304(R)
[22] Bertelsen A, Jorgensen S and Drewsen M 2005 The rotational temperature of polar molecular ions in Coulomb crystals Preprint physics/0504128
[23] Blythe P, Roth B, Fröhlich U, Wenz H and Schiller S 2005 Production of cold trapped molecular hydrogen ions *Phys. Rev. Lett.* at press
[24] Schätz T *et al* 2001 Crystalline ion beams *Nature* **412** 717–20
[25] Fröhlich U, Roth B and Schiller S 2005 Ellipsoidal coulomb crystals in a linear radio-frequency trap *Phys. Plasmas* **12** 073506
[26] Schiller S and Lämmerzahl C 2003 Molecular dynamics simulation of sympathetic crystallization of molecular ions *Phys. Rev.* A **68** 053406(5)
[27] Berkeland D J *et al* 1998 Minimization of ion micromotion in a Paul trap *J. Appl. Phys.* **83** 5025–33
[28] Spears K G and Fehsenfeld F C 1972 Termolecular association reactions of Mg, Ca, and Ba ions *J. Chem. Phys.* **56** 5698
[29] Armentrout P B and Beauchamp J L 1980 Experimental and theoretical studies of the reaction $Ba^+(D_2,D)BaD^+$: sequential impulse model for endothermic reactions *Chem. Phys.* **48** 315
[30] Huber K P and Herzberg G 1979 *Molecular Spectra and Molecular Structure* (New York: Van Nostrand Reinhold)
[31] Johnsen R, Brown H L and Biondi M A 1970 Reactions of Na^+, K^+, and Ba^+ ions with O_2, NO, and H_2O molecules *J. Chem. Phys.* **52** 5080
[32] Hornekær L 2000 Single and multi-species Coulomb ion crystals: structures, dynamics and sympathetic cooling *PhD Thesis* Aarhus University
[33] Barrett M D *et al* 2003 Sympathetic cooling of $^9Be^+$ and $^{24}Mg^+$ for quantum logic *Phys. Rev.* A **68** 042302
[34] Prestage J D *et al* 1991 Dynamics of charged particles in a Paul radio-frequency trap *Phys. Rev. Lett.* **66** 2964–7
[35] Ryjkov V L, Zhao X and Schuessler H 2005 Simulations of the rf heating rates in a linear quadrupole ion trap *Phys. Rev.* A **71** 033414
[36] Gruber L *et al* 2001 Evidence for highly charged ion Coulomb crystallization in multicomponent strongly coupled plasmas *Phys. Rev. Lett.* **86** 636–9
[37] Jensen M J *et al* 2005 Rapid heating of a strongly coupled plasma near the solid–liquid phase transition *Phys. Rev. Lett.* **94** 025001
[38] Baba T and Waki I 2002 Spectral shape of *in situ* mass spectra of sympathetically cooled molecular ions *Japan. J. Appl. Phys.* **92** 4109–16
[39] Roth B, Blythe P, Wenz H and Schiller S 2005 Motional resonance coupling in cold multi-species Coulomb crystals, in preparation